Nanoscale

Accepted Manuscript

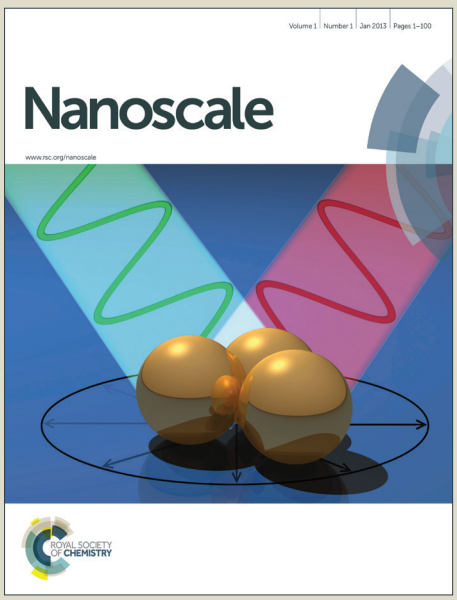

ROYAL SOCIETY OF CHEMISTRY

www.rsc.org/nanoscale

Journal Name

ARTICLE

Excess Titanium Dioxide Nanoparticles on Cell Surface Induce Cytotoxicity by Hindering Ion Exchange and Disrupting Exocytosis Processes

Received 00th January 20xx,
Accepted 00th January 20xx

DOI: 10.1039/x0xx00000x

www.rsc.org/

Yanli Wang,[a]* Chenjie Yao,[a] Chenchen Li,[a] Lin Ding,[a] Jian Liu,[c] Peng Dong,[a] Haiping Fang,[c] Zhendong Lei[b]*, Guosheng Shi,[c]* and Minghong Wu[a,d]*

To date, considerable effort has been devoted to determine the potential toxicity of nanoparticles to cells and organisms. However, determining the mechanism of cytotoxicity induced by different types of nanoparticles remains challenging. Herein, typically low toxicity nanomaterials were used as a model to investigate the mechanism of cytotoxicity induced by low toxicity nanomaterials. We studied the effect of nano-TiO_2, nano-Al_2O_3 and nano-SiO_2 deposition films on the ions concentration on a cell-free system simulating the cell membrane. The results showed that the ions concentration of K^+, Ca^{2+}, Na^+, Mg^{2+} and SO_4^{2-} decreased significantly following filtration of the prepared deposition films. More specifically, at high nano-TiO_2 concentration (200 mg/L) and long nano-TiO_2 deposition time (48 h), the concentration of Na^+ decreased from 2958.01 to 2775.72, 2749.86, 2757.36, and 2719.82 mg/L, respectively, for the four types of nano-TiO_2 studied. Likewise, the concentration of SO_4^{2-} decreased from 38.83 to 35.00, 35.80, 35.40, and 35.27 mg/L, respectively. The other two kinds of typical low toxicity nanomaterials (nano-Al_2O_3 and nano-SiO_2) have a similar impact on the ions concentration change trend. Adsorption of ions on nanoparticles and the hydrated shell around the ions strongly hindered the ions through the nanoparticles films. The endocytosed nanoparticles could be released from the cells without inducing cytotoxicity. Hindering the ion exchange and disrupting the exocytosis process is the main factor that induces cytotoxicity in the presence of excess nano-TiO_2 on the cell surface. The current findings may offer a universal principle for understanding the mechanism of cytotoxicity induced by low toxicity nanomaterials.

Introduction

The development of nanomaterials for biomedical and biotechnological applications is a research area that holds great promise and interest.[1] However, increasing evidence suggests that the special physicochemical properties of nanomaterials pose potential risks to human health. Therefore, considerable effort has been devoted to identify the potential toxicity of nanoparticles to cells and organisms.[2,3] However, to date, determining the characteristics responsible for the hazardous nature of some nanoparticles remains the main challenge, and is a critical issue that will determine future biological applications.[4] The toxicity of nanomaterials remains debatable, as evidenced by current contradicting reports.[5-8] Presently, it is universally believed that there are two factors that determine the onset of cytotoxicity of different types of low toxicity nanomaterials. The first factor relates to the presence of the endocytosed nanomaterial in the cells. The second factor relates to the overloading of the nanomaterial on the cell surface. Many studies demonstrate that the internalization of nanoparticles into cells plays a key role in intercellular response and cytotoxicity.[9–12] However, endocytosis of many nanoparticles will reach saturation depending on incubation time or nanoparticle dosage.[13-17] Cytotoxicity is not observed in low toxicity nanoparticles even at high nanoparticle concentrations of 100 mg/L. Furthermore, nanoparticles, such as TiO_2,[13] silica,[12] Ag,[18] and $Gd@C_{82}(OH)_{22}$,[19] can be released from the cells for a prolonged time. However, the question remains: why is the cytotoxicity behavior of some low toxicity nanoparticles time and/or dose dependent? Some studies demonstrate that the extent of agglomeration of the nanoparticles plays an important role in cytotoxicity responses.[18,20] Wittmaack[21] explained that

[a] Institute of Nanochemistry and Nanobiology, Shanghai University, Shanghai 200444, P.R. China.E-mail: wangyanli@staff.shu.edu.cn
[b] Department of Physics, Tsinghua University, Beijing 100084, P.R. China. E-mail: leizd13@mails.tsinghua.edu.cn
[c] Division of Interfacial Water and Key Laboratory of Interfacial Physics and Technology, Shanghai Institute of Applied Physics, Chinese Academy of Sciences, Shanghai 201800, P.R. China. E-mail:shiguosheng@sinap.ac.cn
[d] School of Environmental and Chemical Engineering, Shanghai University, Shanghai 200444, P.R. China.E-mail:mhwu@shu.edu.cn

Electronic Supplementary Information (ESI) available: Nano-TiO_2 characterization; changes in nucleus morphology; apoptosis assay; variations in Ca^{2+}; schematic of the experiment to simulate ion exchange; TEM images; ion concentration change after filtered through the nano-deposition films; theoretical simulation methods; ROS generation; intercellular communication; the movie shows the process of Na^+ in the films. See DOI: 10.1039/x0xx00000x

suspended silica nanoparticles (NPs) would agglomerate and then settle under gravitational force with time. Cell death was attributed to cell overload with NPs. However, there are no further studies exploring the mechanism of cytotoxicity induced by excessive amounts of NPs on the cell surface.

Titanium dioxide nanoparticles (nano-TiO_2) are manufactured worldwide and commonly applied in many fields.[22,23] Owing to the presence of nano-TiO_2 in a wide variety of products, its toxicology has attracted growing interest in recent years.[24] To date, reports on the toxicity of nano-TiO_2 remain conflicting. Some studies showed that nano-TiO_2 features a low, if not negligible, toxicity.[25-31] In contrast, many other studies indicated that nano-TiO_2 exhibit cytotoxicity and genotoxicity to various cell models such as fibroblasts, macrophages, keratinocytes, epithelial cells, and liver cells.[2,25,32,33] As stated above, the mechanism of cytotoxicity induced by different types of nanoparticles is complex and is yet to be fully understood. Herein, we employed four types of nano-TiO_2 as research models to determine the main mechanism of cytotoxicity induced by low toxicity nanomaterials. Our results showed that overloading of the cell surface with nano-TiO_2, which hinders ion exchange and disrupts exocytosis processes, is the main factor that induces cytotoxicity.

Results and discussion

Characterization of Nano-TiO_2

Nano-TiO_2 is a typical low toxicity nanomaterial. Four types of nano-TiO_2 particles namely, NT (nanotubes, average length 70 nm), NP1 (nanoparticles, average diameter 30 nm), and NP2 and NP3 (nanoparticles, average diameter 50 nm, with different crystal phases and zeta potentials) were examined. The size and morphology of the particles were characterized by transmission electron microscopy (TEM). Fig. 1a-d shows TEM images of the different types of nano-TiO_2 particles examined. The respective detailed size distributions of the particles are shown in Fig. 1e-h that were determined upon assessment of ~400 particles in the TEM images using Image J software. Based on the X-ray diffraction (XRD) patterns (ESI, Fig. S1†), NT featured an amorphous phase, NP3 featured a rutile phase, whereas NP1 and NP2 featured a mixed anatase-rutile phase. The X-ray fluorescence (XRF) analyses revealed that the purity levels of the nano-TiO_2 particles were higher than 95%. The detailed characterization data are summarized in ESI, Table S1†.

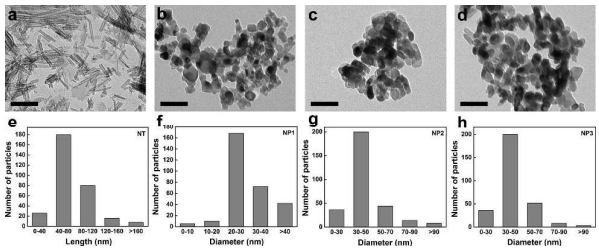

Fig. 1 TEM images and size distribution of nano-TiO_2. (a-d) TEM images of nano-TiO_2: (a) NT; (b) NP1; (c) NP2 and (d) NP3; (e-h) Size distribution histograms of nano-TiO_2: (e) NT; (f) NP1; (g) NP2 and (h) NP3 based on the analysis of ~400 particles using Image J. Scale bar: 200 nm.

Cytotoxicity Studies of Nano-TiO_2

Effect of Excessive Amounts of Nano-TiO_2 on Cell Surface. Based on our results, TiO_2 NPs have similar effect on cytotoxicity at different co-incubation concentrations to three diffenrent cell lines (human gastric epithelial cell line (GES-1), mouse neural stem cells (NSCs) and mouse breast cancer cells (4T1)). We found that the cytotoxicity of TiO_2-NPs was similar in the three cell lines used. (ESI, Fig. S2†). So, we chose one cell line (4TI) as model to investigate the mechanism of TiO_2-NPs induced cytotoxicity. To identify the main factor determining the onset of cytotoxicity, i.e., the presence of nano-TiO_2 in either the cells or on the cell surface, apoptosis and necrosis induced by nano-TiO_2 were compared under two different conditions. Under the first set of experimental conditions, the cells were incubated with nano-TiO_2 for 24 h. After which, excess nano-TiO_2 was removed from the cell surface and the cells were cultured in a fresh medium without nano-TiO_2 for 24 h. Following the second incubation, endocytosis of cells reached saturation. The level of endocytosis of nano-TiO_2 was different following incubation with different concentrations of nano-TiO_2.[13] If nano-TiO_2 in the cells induces cytotoxicity, the normal cell ratios are expected to decrease with increasing nano-TiO_2 incubation concentrations. However, our results showed that following removal of excess nano-TiO_2 from the cell surface, the normal cell ratios remained high i.e., >84.0%, and no dose-dependent trend was observed (Fig. 2). This finding indicates that endocytosed nano-TiO_2 does not induce obvious cytotoxicity regardless of the concentration of nano-TiO_2 in the cells (Fig. 2a–c). In contrast, under the second set of experimental conditions, i.e., incubation of the cells in the presence of excess nano-TiO_2 on the cell surface for 48 h, the resulting apoptosis ratios displayed a dose-dependent behavior. When the concentration of nano-TiO_2 was 200 mg/L, the apoptosis ratio was 31.4% and the normal cell ratio was only 67.7% (Fig. 2d-h). Fig. 2h clearly shows the variations in cytotoxicity induced by nano-TiO_2 under two different conditions, i.e., in the presence and absence of excess nano-TiO_2 on the cell surface. Confocal images (See in ESI Fig. S3†) shows substantial coverage of the cell surface with excess nano-TiO_2 following incubation of the cells in the presence of 200 mg/L nano-TiO_2 for 48 h. Based on these results, we can conclude that the presence of excess nano-TiO_2 on the cell surface is the main factor that induces cytotoxicity.

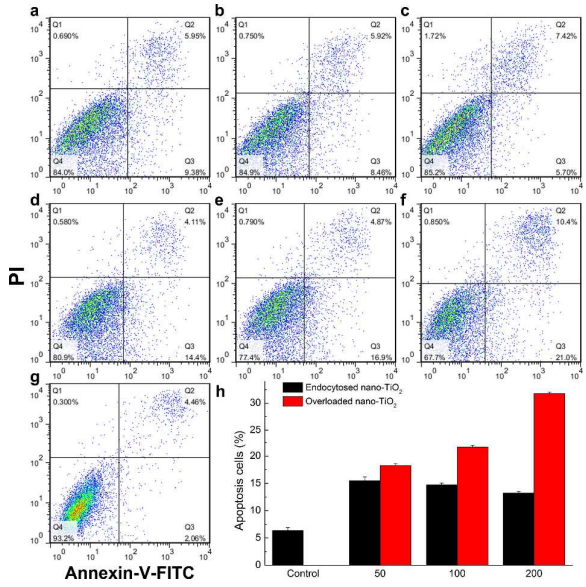

Fig. 2 Flow cytometry results of the annexin V-FITC (fluorescein isothiocyanate) and PI (propidium iodide) assays. Cells that stain strongly for annexin V-FITC$^+$ and PI$^+$ are observed in the upper right quadrant, cells that stain strongly for annexin V-FITC$^+$ and PI$^-$ are observed in the lower right quadrant, whereas cells that stain strongly for annexin V-FITC$^-$ and PI$^-$ are observed in the lower left quadrant. (a-c) Cells were respectively incubated in the presence of 50, 100, and 200 mg/L NP1 for 24 h. Subsequently, excess NP1 was rinsed off, and the cells were incubated in fresh culture medium for another 24 h. (d-f) Cells were incubated with 50, 100, and 200 mg/L NP1 for 48 h. (g) Control group that was incubated in the absence of nano-TiO_2 for 48 h. (h) Apoptosis ratios obtained from annexin V and PI staining.

Effect of High Nano-TiO_2 Concentrations and Long Incubation Time on Cytotoxicity. To evaluate the effect of excess nano-TiO_2 on cytotoxicity, a relationship was determined between variations in the cytotoxicity and nano-TiO_2 amount on the cell surface by testing cell viability and apoptosis. High concentrations and long incubation time in the presence of nano-TiO_2 led to increased amounts of nano-TiO_2 deposited on the cell surface. For the experiments, 4T1 cells were incubated in the presence of nano-TiO_2 at different concentrations (25, 50, 100, 150, 200 mg/L), and cell viability was determined at 24 and 48 h of incubation. The results showed that the considerable reduction in cell viability was dependent on the nano-TiO_2 dosage and incubation time (Fig. 3a, b). The results of the apoptosis and necrosis study further confirmed this finding. As observed in ESI, Fig. S4†, incubation for 48 h in the presence of 200 mg/L nano-TiO_2 led to an approximate three-fold increase in apoptosis when compared with that in the presence of 50 mg/L nano-TiO_2. The generation of reactive oxygen species (ROS) following exposure to nano-TiO_2 was additionally examined (Fig. 3c). A significant level of ROS production was observed following exposure to 200 mg/L nano-TiO_2 for 48 h. As reported, the activation of Ca^{2+} is considered as a contributor to variations in the cell morphology and function associated with apoptosis.[34] As shown in Fig. 3d and ESI, Fig. S5†, increases in the intracellular Ca^{2+} concentration were only induced upon exposure to 200 mg/L nano-TiO_2. These results showed that the cytotoxicity of nano-TiO_2 increased with increasing nano-TiO_2 incubation concentrations and incubation time. Simon *et al.* reported that TiO_2-NPs internalized in cells altered the calcium homeostasis and induced a decrease in cell proliferation associated with an early keratinocyte differentiation, without any indication of cell death.[35] In addition to the conclusion deduced from the results in Fig. 2, we can infer that thicker coverage of excess nano-TiO_2 on the cell surface induce severer cytotoxicity.

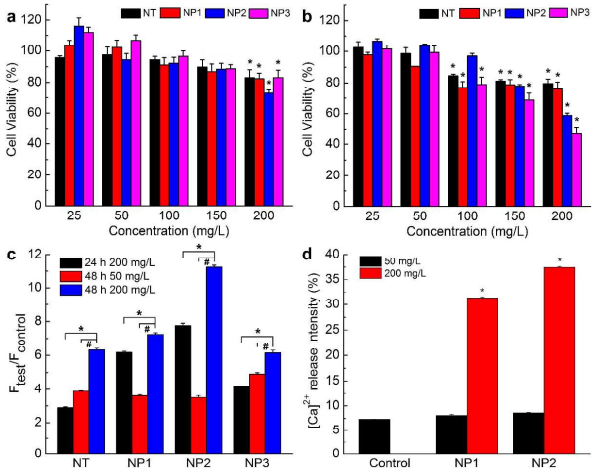

Fig. 3 Cytotoxicity evaluation of Nano-TiO_2. 4T1 cells were cultured in fresh medium after pre-incubating the cells with nano-TiO_2 at different concentrations for 24 and 48 h. (a, b) Cell viability of 4T1 cells using CCK-8 assay. (a) 24 and (b) 48 h. *$p < 0.05$ when compared with the control group. Standard error obtained from five separate experiments. (c) Effect of nano-TiO_2 concentration on ROS generation in 4T1 cells. Notation of data with the square bracket and * indicates significant difference between the 200 mg/L nano-TiO_2-treated groups for 24 and 48 h by one-way analysis of variance (ANOVA), # indicates significant difference between the 50 and 200 mg/L nano-TiO_2-treated groups for 48 h. (d) Flow cytometry results of the variations in the Ca^{2+} concentration.

Release Studies of Endocytosed Nano-TiO_2 from Cells. Considering that endocytosed nano-TiO_2 particles do not induce obvious cytotoxicity, the fate of the nanoparticles was assessed by investigating the intracellular transport process in the cells. 4T1 cells were incubated in the presence of 20 mg/L fluorescein isothiocyanate (FITC)-labeled NP1 (FITC-NP1). Then, the dynamics of FITC-NP1 in the cells over a time period of 4-48 h was examined using confocal microscopy (Fig. 4). After 4 and 8 h incubation, FITC-NP1 gradually internalized into the cells and accumulated in the cytoplasm (Fig. 4a, b). Few yellow fluorescence spots appeared for the first time in the lysosomes after 12 h of incubation (Fig. 4c). Subsequently, an increasing number of FITC-NP1 particles were internalized into the cells and transported to the lysosomes with prolonged incubation time (Fig. 4d, e). Most of the internalized FITC-NP1 ultimately entered the lysosomes of 4T1 cells at 48 h of incubation.[11] Our former study showed that lysosomes containing nano-TiO_2 would move towards the cellular membrane, recycle at the cell surface, and finally exocytose from the cells.[13] Based on our results, we can infer that the endocytosed nanoparticles can be released from the cells without inducing any cytotoxicity in the

absence of excess nanoparticles on the cell surface that otherwise disrupts the exocytosis process.

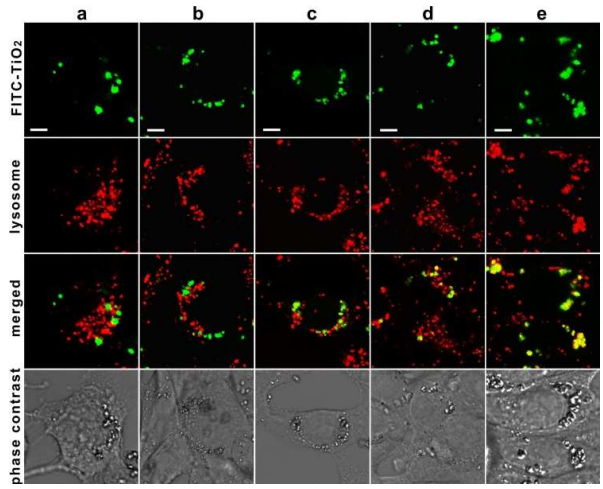

Fig. 4 Subcellular localization of FITC-labeled NP1 in 4T1 cells. The fluorescent and phase contrast images of 4T1 cells were obtained using a laser scanning confocal microscope. The green and red spots show the intracellular distribution of FITC-NP1 and the lysosomes, and the yellow spots indicate colocalization of FITC-NP1 and the lysosomes. Cells were exposed to 10 mg/L FITC-NP1 for different time of (a) 4; (b) 8; (c) 12; (d) 24 and (e) 48 h. Scale bar: 5 μm.

Mechanism of Cytotoxicity Induced by the Presence of Excess Nano-TiO_2

Effect of Nano-TiO_2, Nano-Al_2O_3 and Nano-SiO_2 Deposition Films on Ions Exchange Rate. To study the influence of the presence of excess nanoparticles on cytotoxicity and determine the corresponding mechanism, the effect of nano-TiO_2 deposition film on the ion exchange of the excess nanoparticles on the cell surface was examined. The experimental process is schematically illustrated in ESI, Fig. S6†. The presence of K^+, Ca^{2+}, Na^+, Mg^{2+} and SO_4^{2-} in Hank's solution following filtration of the nano-TiO_2 deposition films was assessed. Hank's solution was used to simulate the nutrient medium because it contains several metal ions that are typically present in organisms. Ions K^+, Ca^{2+}, Na^+ Mg^{2+} and SO_4^{2-} are present in the cells and play key roles in normal cell functions.[36-39] Interestingly, the ion concentration decreased significantly following filtration of the nano-TiO_2 deposition films. Particularly, for films (i.e., NT, NP1, NP2, and NP3) prepared in the presence of high nano-TiO_2 concentrations (200 mg/L) and long nan-TiO_2 deposition time (48 h), the concentration of Na^+ decreased from 2958.01 to 2775.72, 2749.86, 2757.36, and 2719.82 mg/L, respectively. Likewise, the concentration of SO_4^{2-} decreased from 38.83 mg/L to 35.00, 35.80, 35.40, and 35.27 mg/L, respectively (Fig. 5). The inhibition ratio analysis results are shown in Fig. 6. For all kinds of ion, the inhibition ratios are all in a time- and dose-dependent manner. For instance, in NP1-treated groups, the inhibition ratio of Na^+ was 25.62% after being filtered through the 200 mg/L NP1

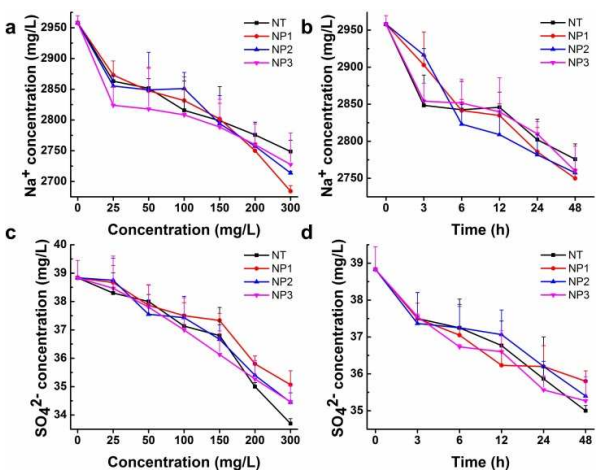

Fig. 5 Variations in the ion concentration as a function of nano-TiO_2 deposition time and nano-TiO_2 concentration following filtration of the nano-TiO_2 films: changes in the concentration of Na^+ as a function of (a) nano-TiO_2 concentration and (b) deposition time of nano-TiO_2 films, and changes in the concentration of SO_4^{2-} as a function of (c) nano-TiO_2 concentration and (d) deposition time of nano-TiO_2 films.

deposition films for 3 h. With the deposition time prolonging to 48 h, the inhibition ratio of Na^+ increased to 62.16%. When the deposition concentration of NP1 increased from 25 mg/L to 300 mg/L, the inhibition ratio of Na^+ increased from 29.45% to 66.09%. The variation tendencies of all kinds of ions are all in a similar way. Furthermore, the variations in the ion concentrations were dependent on the nano-TiO_2 deposition time and nano-TiO_2 concentration regardless of the type of ion. Some differences in the extent of ion concentration variations were observed, though a general decreasing trend was obtained (ESI, Fig. S7†). For instance, the concentration of K^+, Ca^{2+} and Mg^{2+} decreased from 212.70, 49.41 and 10.23 mg/L to 200.64, 44.76 and 9.63 mg/L, after filtrated of the NP1 deposition films of high NP1 concentrations (200 mg/L) and long NP1 deposition time (48 h), respectively. Further, we investigate the effect of nano-Al_2O_3 and nano-SiO_2 on the ions concentration. The characterization data of nano-Al_2O_3 and nano-SiO_2 used in this study are shown in ESI, Fig. S8†. The results show that nano-Al_2O_3 and nano-SiO_2 have a similar impact on the ions concentration change trend (ESI, Fig. S9† and Fig. S10†) and inhibition ratio (ESI, Fig. S11†). The concentration of K^+, Ca^{2+}, Na^+, Mg^{2+} and SO_4^{2-} decreased from 248.67, 53.88, 3524.23, 11.78 and 54.25 mg/L to 222.42, 47.41, 3337.21, 10.37 and 44.7 mg/L, after being filtrated of the S1 deposition films of high S1 concentrations (200 mg/L) and long S1 deposition time (48 h), respectively. Similarly, for A1, the concentration of K^+, Ca^{2+}, Na^+, Mg^{2+} and SO_4^{2-} decreased to 221.69, 47.46, 3148.91, 10.68 and 45.25 mg/L, after filtrated of the A1 deposition films of high A1 concentrations (200 mg/L) and long A1 deposition time (48 h), respectively. For inhibition ratios, in S1-treated groups, the inhibition ratio of Na^+ decreased from 20.58% to 48.94% after being filtered through the 200 mg/L S1 deposition films from 3 h to 24 h. When the deposition concentration of S1 increased from 25 mg/L to 300 mg/L, the inhibition ratio of Na^+ increased

from 15.57% to 66.00%. In A1-treated groups, the inhibition ratio of Na^+ decreased from 16.89% to 55.68% after being filtered through the 200 mg/L A1 deposition films from 3 h to 24 h. When the deposition concentration of A1 increased from 25 mg/L to 300 mg/L, the inhibition ratio of Na^+ increased from 14.83% to 56.22%. This indicated that there was no any specific mechanism of different kinds of low toxicity nanomaterials on the effect of ions concentration.

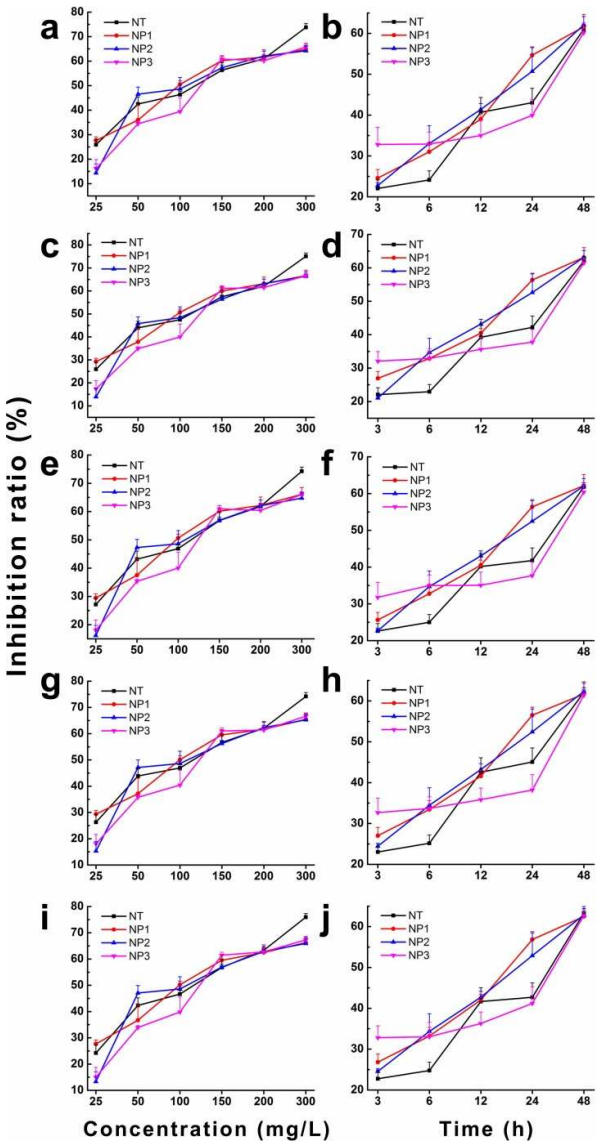

Fig. 6 Inhibition ratio of (a, b) K^+; (c, d) Ca^{2+}; (e, f) Na^+; (g, h) Mg^{2+} and (i, j) SO_4^{2-} following filtration of the nano-TiO_2 films for 5 min using Hank's solution. The films were prepared via deposition of (a, c, e, g, i) varying amounts of nano-TiO_2 for 48 h and (b, d, f, h, j) 200 mg/L at varying deposition time.

Two reasons may induce the hindering of ions for low toxicity nanoparticles, one is the adsorption of ions on nanoparticles. For insoluble nanoparticles, the adsorption property was involved in cellular influences. It is well known that NPs surfaces are modified by the adsorption of biomolecules such as proteins in a biological environment.[40-43] Based on our result, the serum in the cell culture medium has big infulence on the adsorption ability of nano-TiO_2 (ESI, Fig. S12†). The ions concentrations following filtration of the prepared deposition films with FBS decreased more significantly than without FBS treated group. This indicates that the interaction between FBS and nano-TiO_2 have great effect on ions concentration changes. This adsorption ability leads to cytotoxic activity.[44,45]

Molecular dynamics (MD) simulations study results show that the hydrated shell around the ions strongly influenced the ions through the channel in the nanoparticles films, thereby restricting diffusion of the ions across the films when compared with simple water molecules (Movie S1). This is the other main reason for the hindering of ions with three kinds of low toxicity nanoparticles. Two systems with different relative distances between the hole in the nanoparticles films and ion channels in the phospholipid membrane were simulated to illustrate the impact upon deposition of the nanoparticles films on the cell surface. The setup of one system (AA-stacked model) is shown in Fig. 7a, whereby the hole in the nanoparticles is located on the ion channel in the phospholipid membrane. The second system (AB-stacked model) is shown in ESI, Fig. S13†, whereby the hole in the nanoparticles is located on the phospholipid molecules in the phospholipid membrane. The rate of flow of water and ions was calculated under a pressure difference of 100 MPa. For both models, the flow of both water and ions were comparable. This result indicated that the different distribution of the holes in nanoparticles of different shapes or sizes in the membrane minimally influenced the ion exchange process, as consistent with the experimental results (Fig. 5). Ion inhibition ratios were calculated by the rate of ions and water molecules crossing the films in the simulation studies as follows: $R = (1 - r_{ion}/r_{water}C_{ion}) \times 100\%$, where r_{ion} is the ion flow, r_{water} is the water flow, and C_{ion} is the ion concentration. The Na^+ inhibition ratios of both systems are shown in Fig. 7c. The Na^+ inhibition ratios are ~80% by the nanoparticle films (Fig. 7c).

These results demonstrated that the nano-TiO_2 deposition films can hinder ion exchange. Dysfunction of Na^+, K^+-ATPase is known to reduce K^+ uptake, leading to a considerable loss of cellular K^+ and likelihood of apoptosis of many cell types.[39] Calcium ion channels regulate cellular functions including endo- and exocytosis and gene expression.[36] Cousin et al. showed that a mean 15% inhibition of Ca^{2+} entry could cause a 39% inhibition of exocytosis.[37] It has also been reported that Na^+/K^+-ATPase inhibitors can disturb the Na^+ and K^+ exchange processes and inhibit cell–cell fusion.[38]

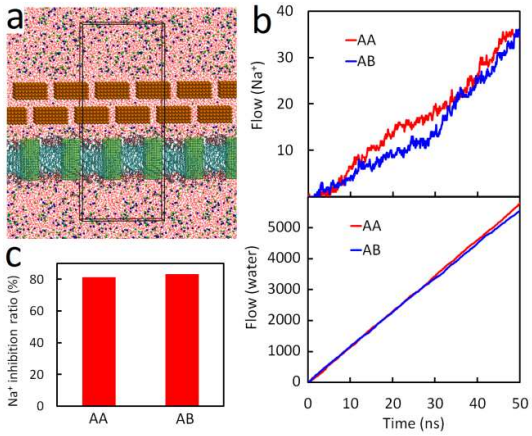

Fig. 7 Molecular dynamics simulations on the effect of nano-TiO_2 deposition films of ions exchange. (a) Snapshot of NaCl solution flow through the nanoparticle film (AA-stacked model is shown as an example). Na^+ and Cl^- ions and nanoparticles are shown as blue, green, and yellow spheres, respectively, and water molecules are represented by the red lines. Lipids (hydrogen atoms not shown) are represented by the cyan lines and trans-membrane ion channels are located within the lime spheres. (b) Variations in the flow of Na^+ and water molecules through the nanoparticle films and phospholipid membrane as a function of simulation time. The slope of the curve represents the flow rate. (c) Na^+ inhibition ratios obtained for the two AA- and AB-stacked models studied.

Effect of Excess Nano-TiO_2 on Cell Surface on the Exocytosis of Cells. To further evaluate if the hindering of ion exchange by excess nano-TiO_2 would disrupt the exocytosis process, we assessed the function of lysosomes and microtubules, and cell-cell communication. The fusion of the lysosomal membrane with the plasma membrane can result in the release of lysosomes from the cells.[12] The onset of fusion can be determined by measuring the release of β-hexosaminidase, an enzyme that resides in lysosomes, in the culture medium. The enzyme assays for the release of β-hexosaminidase revealed that the 4T1 cells incubated in the presence of 200 mg/L nano-TiO_2 for 4, 8, or 12 h showed no lysosomal destabilization when compared with the control groups. In contrast, after 24 and 48 h of incubation, the release of lysosomal contents in the culture medium increased significantly (Fig. 8). Sohaebuddin *et al.*[2] found that multi-walled carbon nanotubes caused pronounced lysosomal membrane destabilization by releasing lysosomal contents in the cytoplasm. Thus, our results suggested that the presence of cell surface coverage with excess nano-TiO_2 significantly disrupted lysosome exocytosis function. Microtubules function as tracks in material transportation within cells. Accordingly, microtubule damage will suppress material transport in the cells. As observed from Fig. 9, incubation in the presence of nano-TiO_2 at high concentrations and long incubation time interfered with microtubule polymerization and subsequent microtubule function. This finding further confirmed that the presence of excess nano-TiO_2 on the cell surface hinders ion exchange and disrupts the exocytosis process, consequently inducing cytotoxicity.

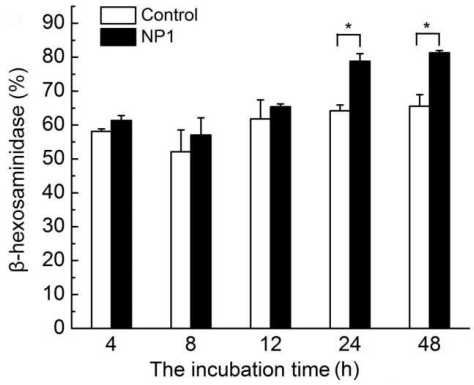

Fig. 8 Release of β-hexosaminidase from the cells following exposure to 200 mg/L NP1 for different time. *p < 0.05 when compared with the control group.

The results showed that the presence of excess nano-TiO_2 significantly influenced ion exchange, consequently hindering communication between the cells and medium. Additionally, herein, we investigated the effect of the presence of excess nano-TiO_2 on the cell-cell communication. Gap junction intracellular communication (GJIC), induced by the connexin protein family, plays an important role in maintaining homeostasis and preventing cell transformation. Among all the connexins, Connexin 43 (Cx43) is one of the widely studied connexins, which is involved in gap junction channel formation, permeability, and turnover.[46] Deng *et al*. found that Ag nanoparticles induced up-regulation of Cx43 protein resulting in the increase of GJIC activity in A549 cells.[47] However, carbon or silica-based nanoparticles showed loss of GJIC in rat lung epithelial cells.[48] Therefore, in this study, we examined the influence of FITC-NPs on the distribution and expression of Cx43 at the plasma membrane. Immunohistochemical staining images of 4T1 cells after treatment with FITC-NP1 and FITC-NP2 (10 and 50 mg/L) for 48 and 24 h are shown in Fig. 10 and ESI, Fig. S14†, respectively. Treatment with FITC-NPs at low concentrations did not affect the cell-to-cell communication. In contrast, when the concentration increased to 50 mg/L, which led to increased expression levels and a wider distribution of the Cx43 protein, considerable changes in the distributing pattern of Cx43 at 48 h were observed (Fig. 10). The average fluorescent intensity of immunostained Cx43 is summarized in Fig. 10f and 10g.

Based on all the results, we can confirm that the presence of excess nanoparticles on the cell surface is the major trigger of cytotoxicity, which hinders ion exchange among cells and between cells and medium, subsequently disrupting the exocytosis process. The endocytosed nanoparticles can be released from cells. If coverage of excess nanoparticles on the cell surface is not thick enough to disrupt the ion exchange rate, no toxicity is induced. Increasing the incubation time and nano-TiO_2 concentration can generate sufficiently thick nano-TiO_2 coverage on the cell surface to influence the ion exchange process, consequently inducing cytotoxicity.

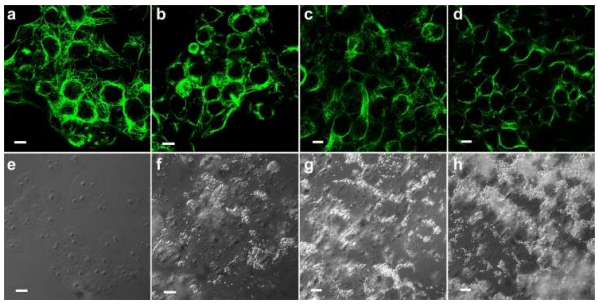

Fig. 9 Microtubule dynamics following exposure with NP1 using immunofluorescence staining: (a–d) fluorescent images of 4T1 cells examined under a laser scanning confocal microscope and (e–h) phase contrast images of 4T1 cells. (a, e) Control group (treated in the absence of nano-TiO_2); groups treated with (b, f) 200 mg/L NP1 for 24 h; (c, g) 50 mg/L NP1 for 48 h, and (d, h) 200 mg/L NP1 for 48 h. Scale bar: 10 μm.

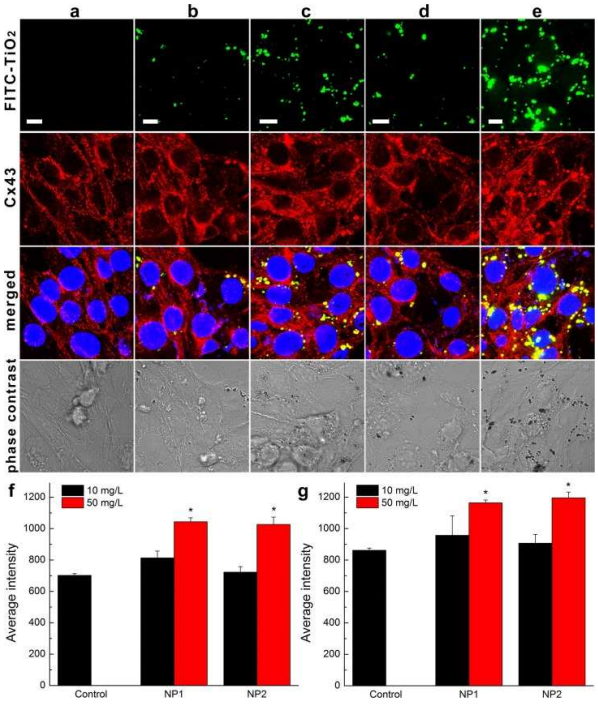

Fig. 10 Fluorescent images of 4T1 cells immunostained with Cx43 monoclonal antibodies: (a) control (treated in the absence of nano-TiO_2); (b, c) cells incubated with 10 and 50 mg/L FITC-NP1 for 48 h; (d, e) cells incubated with 10 and 50 mg/L FITC-NP2 for 48 h. Analysis of average fluorescent intensity of immunostained Cx43 in 4T1 cells following incubation with FITC-NP1 and FITC-NP2 (10 and 50 mg/L) for (f) 24 and (g) 48 h, respectively. Scale bar: 10 μm.

The cytotoxicity of nano-TiO_2 induced by ion exchange hindering results in reduced cell viability, increased Ca^{2+} concentration, ROS generation, lysosomal destabilization, microtubule polymerization, and intercellular communication that is dependent on the incubation time and nano-TiO_2 dose. The present findings may offer a general principle for understanding the mechanism of cytotoxicity induced by low toxicity nanomaterials. Our results are consistent with many earlier literature studies regarding the cytotoxicity of low toxicity nanoparticles as exemplified. For low toxicity nanoparticles, such as SiO_2,[49-51] aluminum oxide,[52] and TiO_2[52-54] nanoparticles, cytotoxicity was observed at high nanoparticle concentrations. Ware *et al.*[55] confirmed that polyethylenimine-coated quantum dots endocytosed in cells and were encapsulated in the membrane-bound vesicles. When endocytosis reached saturation, particles would accumulate on the membrane and the level of cell death would decrease. Mu *et al.*[49] found that exposure of cells with 100 μg/mL silica NPs for 24 h resulted in the lysis of most of the cells, with large clumps of silica particles visible in the debris. This finding indicated that a high amount of silica NPs deposited on the cell membrane by gravitational settling.

Experimental Section

Samples of Three Kinds of Low Toxicity Nanomaterials

Four types of nano-TiO_2 samples were used in this study namely, NT (nanotubes, average length 70 nm); NP1 (nanoparticles, average diameter 30 nm); NP2 (nanoparticles, average diameter 50 nm) and NP3 (nanoparticles, average diameter 50 nm). NP1 and NP2 were purchased from Wanjing Co. Ltd. (China) and Degussa Co. Ltd. (Germany), respectively. NP3 was kindly provided by the Nano-Science and Technology Research Center of Shanghai University. NT was synthesized according to the method described elsewhere. Besides, two types of nano-SiO_2 and nano-Al_2O_3 were also used, namely, S1 (nano-SiO_2, average diameter 30 nm); S2 (nano-SiO_2, average diameter 20 nm); A1 (nano-Al_2O_3, average diameter 40 nm) and A2 (nano-Al_2O_3, average diameter 20 nm). These nanoparticles were all purchased from Wanjing Co. Ltd. (China). Stock solutions of all kinds of nanoparticles were prepared by dispersing the nanoparticles sample in deionized water at a concentration of 1000 mg/L. The treated suspension cells were freshly prepared prior to the experiments by diluting the above-prepared stock solution in the culture medium to achieve a predetermined concentration.

Characterization of Nanoparticles

The purity of the nano-TiO_2 samples was assessed by X-ray fluorescence spectroscopy (XRF; S4-Explorer, Bruker, Germany). XRD (Rigaku Co., Tokyo, Japan) was used to determine the crystal phase of the nano-TiO_2 samples. The shape and size of the nano-TiO_2, nano-Al_2O_3 and nano-SiO_2 samples were investigated by TEM (JEM-200CX, JEOL, Japan). The size distribution of the nanoparticles was computed using Image J software based on the analysis of more than 400 particles. The hydrodynamic size of the nano-TiO_2 particles in water and culture medium and their zeta potential in water were measured on a Nanosizer (Zetasizer 3000 HS, Malvern, UK). The Brunauer–Emmett–Teller (BET) surface area of the nano-TiO_2 samples was determined on an ASAP 2020 M+C (Micromeritics Instruments Company, USA).

Preparation of Deposition Films and Their Effect on Ion Exchange

To study the effect of nanoparticle deposition film on ion exchange, the following experiment was conducted, as schematically illustrated in (ESI, Fig. S6†). Briefly, 0.22-μm pore-sized filter membranes were used to simulate the cellular membrane. The filter membranes were incubated in the presence of nano-TiO_2 (NT, NP1, NP2, or NP3), nano-Al_2O_3 and nano-SiO_2 at different concentrations of 25, 50, 100, 150, 200, and 300 mg/L for 48 h, or 200 mg/L nanoparticles for different incubation time of 3, 6, 12, 24, and 48 h to achieve nanoparticles loading of the membrane by gravitational force. Then, the deposition films were carefully removed and transferred to a filter device. Hank's solution was used to simulate the nutrient medium because it contains several metal ions that are typically present in organisms. Hank's solution (20 mL) was passed through the nanoparticle deposition films via filtration for 5 min. The filtered solution was then collected. The concentration of K^+, Ca^{2+}, Na^+ and Mg^{2+} was determined by inductively coupled plasma atomic emission spectroscopy (ICP-AES; LeemanLabs., USA), whereas the concentration of SO_4^{2-} was determined by ion chromatography (IC; Metrohm China Ltd, China). Results were expressed in ion concentration and ion inhibition ratio, and three independent experiments were performed.

The ion inhibition ratio of K^+, Ca^{2+}, Na^+, Mg^{2+} and SO_4^{2-} was calculated according to the following formula:

$$I = \text{Ion passing rate (mg/min)} = \frac{C_{ion} \times V}{T}$$

$$\text{Ion inhibition ratio (\%)} = \frac{I_{control} - I_{ion}}{I_{control}} \times 100\%$$

Where C_{ion} represents the concentration of filtered Hanks' solution through nano-TiO_2 deposition films; V represents the filtration volume; T represents the filtration volume; $I_{control}$ represents the ion passing rate of control group; I_{ion} represents the ion passing rate of experimental group.

Theoretical Simulation Methods

Hydrophilic nano-TiO_2 was constructed by orthogonal packing of 500 beads (10×10×5), with lattice dimensions of 2.294 Å × 2.953 Å × 2.953 Å to mimic the structure of TiO_2 rutile. Three systems were constructed, with two, four, or six layers of nanoparticles including two nanoparticles per layer (the width of both the horizontal and vertical channels was 10 Å). Periodic boundaries were employed to form a continuous two-dimensional laminate membrane. The laminates were solvated with >20-Å-thick layers of salt solution on both sides, with a constant NaCl/water ratio of 1:32. All MD simulations were performed using the NAMD2.9/VMD1.9 package[56,57] with the CHARMM27 force field[58] and TIP3P water model.[59] The TiO_2 beads were modeled as uncharged Lennard–Jones particles with parameters of $R_{min/2}$ = 2.0 Å and ε = 0.13 kcal/mol, mimicking the hydrophilicity of TiO_2 (water contact angle of ~ 72°) according to our previous study (ESI, Fig. S13†).[60]

Chemicals and Cell Culture

All chemicals were commercially available. Roswell Park Memorial Institute-1640 (RPMI 1640) cell culture medium and fetal bovine serum were purchased from Invitrogen, California, USA. 4T1 cells (a mouse breast cancer cell line) were provided from the Chinese Academy of Sciences. Cells were grown to confluence in 25-cm^2 flasks supplemented with high-glucose RPMI 1640 and 10% fetal bovine serum, and incubated in a humidified incubator with 5% CO_2 and 95% air at 37 °C. Eighty percent of confluent cells was used in all the assays.

Annexin V-FITC and PI Assays

The annexin V-FITC and PI assays were employed to detect apoptotic and necrotic cells. The procedure used was in accordance with the instructions provided in the annexin V-FITC apoptosis detection kit I (Catalog No. 556547, BD Biosciences, USA). To detect apoptosis of the endocytosed and excess nano-TiO_2, cell incubation was performed in the presence of 50, 100, or 200 mg/L NP1 for 48 h. For the endocytosed NP1, 4T1 cells were incubated with NP1 for 24 h. Then, excess NP1 was washed, and cells were incubated for another 24 h. For the excess NP1, cells were incubated with NP1 for 48 h. Then, annexin V-FITC and PI assays were employed. For the assay, 100 μL 4T1 cells was transferred to a 5 mL culture tube and added to 5 μL FITC-conjugated annexin V (annexin V-FITC) and 5 μL PI at room temperature. After incubation for 15 min at room temperature in the dark, the stained 4T1 cells were diluted with binding buffer and directly analyzed by flow cytometry (FACS, FACS Calibur).

Fluorescent Labeling of Nano-TiO_2

The nano-TiO_2 surfaces were functionalized with primary amines. (3-Aminopropyl) triethoxysilane (APTS) was used to attach the alkoxy silane groups to the surface hydroxyls. The amines were available for the attachment of FITC molecules. For the functionalization, 4 mg nano-TiO_2 was dispersed in 3 mL anhydrous dimethylformamide (DMF). A solution of 0.5 μL APTS diluted in 25 μL DMF was added to the nano-TiO_2 suspension, sonicated, and stirred under nitrogen at room temperature for 20 h. The modified nano-TiO_2 particles were collected by centrifugation (3000 rpm, 15 min) to remove the supernatant. After washing, the modified nano-TiO_2 particles were resuspended in 0.5 mL DMF and mixed with a solution of 1 mg FITC and 0.5 mL DMF. The suspension was stirred for 4 h, and the FITC-labeled nano-TiO_2 particles were collected by centrifugation. After thorough washing of the labeled materials with DMF, the nano-TiO_2 particles were dried under vacuum to remove the organic solvent and stored as dry powders.

Confocal Study of the Subcellular Location and Transportation of Nano-TiO_2

To investigate the subcellular location and transportation of nano-TiO_2 in 4T1 cells, the cells were treated with 10 mg/L FITC-labeled NP1 at 37 °C for varying time (4, 8, 12, 24, and 48 h). Then, the cells were stained by LysoTracker (Invitrogen) to investigate the

contribution of lysosomes to the trans-cellular process of FITC-labeled NP1.

Cell Viability Assays of Nano-TiO_2

Cell viability assays were performed using a CCK-8 Kit (Dojindo Laboratories, Japan) following manufacturer instructions. Cell viability was expressed as the percentage of viable cells in total cells. 4T1 cells were seeded in 96-well plates (5×10^3 cells per well), pre-cultured in culture medium containing different concentrations of nano-TiO_2 for 24 or 48 h. To determine cell viability, each well was treated with CCK-8 Kit according to the manufacturer's instruction and the absorbance of the solution in each well was measured at 450 nm using a Microplate Reader (Thermo, USA).

β-Hexosaminidase Assay

Cells were seeded in a six-well plate at a confluency of 3×10^5 cells per well overnight. Then, the medium was withdrawn from the wells. Fresh medium was added to the wells after the cells were washed with phosphate-buffered saline (PBS). The cells were incubated for 4, 8, 12, 24, or 48 h with or without NP1. The medium (supernatant) was collected and the cells were lysed with 0.1% Triton-X 100 in medium. β-Hexosaminidase assay was performed in a 96-well plate by mixing 50 μL of 2 mg/mL 4-nitrophenyl N-acetyl-β-D-galactosaminide in 0.1 M citrate buffer (pH 4.5) with 75 μL supernatant or cell lysate and incubating for 1 h at 37 °C. After incubation, 100 μL of 0.2 M borate buffer (pH 9.8) was added to the mixture to stop the reaction. The absorbance was measured at 405 nm using a plate reader. Percentage values were obtained by dividing the reading obtained from the supernatant with that of the cell lysate.

Measurement of Ca^{2+} Concentration

First, 4T1 cells were treated with NP1 or NP2 (50 or 200 mg/L) for 48 h. To study the intracellular calcium concentration, the cells were loaded with 10 μM Fluo-3 AM (Beyotime) for 30 min at 37 °C, followed by washing with Dulbecco's PBS three times. Then, the cells were incubated for another 20 min to ensure complete cleavage of Fluo-3 AM upon release of Fluo-3 before illumination by intracellular ester enzyme. Subsequently, the stained 4T1 cells were directly analyzed by flow cytometry (FACS, FACSCalibur, BD Biosciences).

Immunofluorescence Staining of Microtubules

The assay was performed according to the procedure set out in the microtubules immunofluorescence staining kit I (Catalog GMS10278, GMN-MED, USA). 4T1 cells, which grew to ~50% confluence on 22-mm^2 cover slips, were treated with NP1 (50 and 200 mg/L) for 24 and 48 h. Then, the cells were rinsed with PBS and fixed with 4% paraformaldehyde for 15 min at room temperature, rinsed three times with PBS, and permeabilized in 0.2% Triton X-100 for 10 min. The cells were blocked in 2% bovine serum albumin in PBS for 1 h, then incubated with a primary antibody for 30 min at 37 °C. After incubation with a primary antibody, the cells were washed three times with PBS and then incubated with a secondary antibody for 30 min at 37 °C. Nuclei were detected with 4,6-diamidino-2-phenylindole (DAPI). After the final washing step, the cover slips were mounted and slides were visualized using a confocal microscope (FV1000, Olympus Corp., Tokyo, Japan) at 488 nm excitation.

Immunofluorescence Staining of Cx43

4T1 cells were treated with FITC-NP1 and FITC-NP2 (10 and 50 mg/L) for 24 and 48 h. Then, the cells were rinsed with PBS and fixed with 4% paraformaldehyde for 15 min at room temperature, rinsed three times with PBS, and permeabilized in 0.2% Triton X-100 for 10 min. Cells were blocked in 2% bovine serum albumin in PBS for 1 h, then incubated with a rabbit polyclonal anti-Cx43 (1:200, Sigma-Aldrich) primary antibody overnight at 4 °C. After incubation with a primary antibody, cells were washed three times with PBS and then incubated with a goat anti-rabbit antibody conjugated to Alexa Fluor 594 (1:100, Molecular Probe) for 30 min at 37 °C. Nuclei were detected with DAPI. After the final washing step, the cover slips were mounted and slides were visualized using a confocal microscope.

Measurement of ROS after Nano-TiO_2 Exposure

4T1 cells were cultured in 25-cm^2 flasks in the presence of culture medium containing different types of nano-TiO_2 at a final concentration of 50 or 200 mg/L for 24 or 48 h. These cells were subsequently collected and incubated in 2 mL 2′,7′-dichlorodihydrofluorescein diacetate (H_2DCFDA, Invitrogen), a fluorogenic probe commonly used to detect intracellular generation of ROS at 37°C for 40 min. The fluorescence data of oxidized H_2DCFDA were recorded using a Microplate Reader (Thermo) with excitation and emission wavelengths set at 485 ± 20 nm and 535 ± 25 nm, respectively.

DNA Fluorescent Staining and Confocal Laser Scanning Microscopy Studies

Fluorescent probe DAPI is a popular nuclear counterstain that is used in multicolor fluorescent techniques. It stains nuclei specifically, with little or no cytoplasm labeling. 4T1 cells were pre-cultured in culture medium containing 200 mg/L NP1 for 48 h. Then, the cells were collected and sequentially washed with PBS and DAPI (Invitrogen) working solutions. The cells were then kept in 2 mg/L DAPI working solution for 15 min in the dark at room temperature. Finally, the cells were washed twice with PBS to remove excess DAPI and examined under a confocal microscope (FV1000, Olympus Corp., Tokyo, Japan) at 405 nm excitation.

Statistical Analysis

Results were expressed as mean ± standard deviation (SD). Comparisons among the groups were evaluated by *t*-test or ANOVA followed by the Student-Newman-Keuls test. A value of $p < 0.05$ was considered statistically significant.

Conclusions

In summary, we studied the mechanism of cytotoxicity induced by low toxicity nanomaterials. Based on the results of the effect of three kinds of low toxicity nanomaterials deposition film on the ions concentration and volume combined with molecular dynamics simulations study, we inferred that adsorption of ions on nanoparticles and the hydrated shell around the ions strongly hindered the ions through the nanoparticles films which influenced ion exchange among cells and between cells and medium, subsequently disrupting the exocytosis process. The endocytosed nanoparticles could be released from the cells without inducing cytotoxicity. Excess nanoparticles on the cell surface are the major trigger of cytotoxicity. Hindering the ion exchange and disrupting the exocytosis process by excess nanoparticles resulted in reduced cell viability, accelerated increased Ca^{2+} concentrations, reactive oxygen species generation, lysosomal destabilization, microtubule polymerization, and intercellular communication in a time- and dose-dependent manner in the presence of excess nano-TiO_2 on the cell surface. The present results are expected to further clarify the cytotoxicity mechanism of low toxicity nanomaterials.

Acknowledgements

This work was financially supported by the National Basic Research Program of China (973 Program; Grant No. 2011CB933402), National Natural Science Foundation of China (Grant Nos. 21371115, 41430644, 21101104, 40830744, 11404361, and 11025526), Innovation Program of Shanghai Municipal Education Commission (Grant No. 14YZ025), Program for Innovative Research Team in University (Grant No. IRT13078), and the Shanghai Natural Science Foundation of China (Grant No. 13ZR1447900).

References

1 K. Kostarelos, L. Lacerda, G. Pastorin, W. Wu, S. Wieckowski, J. Luangsivilay, S. Godefroy, D. Pantarotto, J. P. Briand, S. Muller, M. Prato and A. Bianco, *Nat. Nanotechnol.,* 2007, **2,** 108-113.
2 S. K. Sohaebuddin, P. T. Thevenot, D. Baker, J. W. Eaton and L. P. Tang, *Part. Fibre Toxicol.,* 2010, **7,** 17.
3 Y. L. Wang, L. L. Yuan, C. J. Yao, L. Ding, C. C. Li, J. Fang, K. K. Sui, Y. F. Liu and M. H. Wu, *Nanoscale,* 2014, **6,** 15333-42.
4 J. N. Qiu, *Nature,* 2012, **489,** 350-350.
5 Y. Guichard, J. Schmit, C. Darne, L. Gate, M. Goutet, D. Rousset, O. Rastoix, R. Wrobel, O. Witschger, A. Martin, V. Fierro and S. Binet, *Ann. Occup. Hyg.,* 2012, **56,** 631-644.
6 S. Arora, J. M. Rajwade and K. M. Paknikar, *Toxicol. Appl. Pharmacol.,* 2012, **258,** 151-165.
7 T. Z. Tong, C. T. T. Binh, J. J. Kelly, J. F. Gaillard and K. A. Gray, *Water. Res.,* 2013, **47,** 2352-2362.
8 J. Y. Zhang, W. H. Song, J. Guo, J. H. Zhang, Z. T. Sun, L. Y. Li, F. Ding and M. L. Gao, *Toxicol. Ind. Health.,* 2013, **29,** 523-533.
9 K. Saha, S. T. Kim, B. Yan, O. R. Miranda, F. S. Alfonso, D. Shlosman and V. M. Rotello, *Small,* 2013, **9,** 300-305.
10 X. E. Jiang, C. Rocker, M. Hafner, S. Brandholt, R. M. Dorlich and G. U. Nienhaus, *ACS Nano,* 2010, **4,** 6787-6797.
11 B. He, Z. R. Jia, W. W. Du, C. Yu, Y. C. Fan,W. B. Dai, L. Yuan, H. Zhang, X. Q. Wang, J. C. Wang, X. Zhang and W. Zhang, *Biomaterials,* 2013, **34,** 4309-4326.
12 R. E. Yanes, D. Tarn, A. A. Hwang, D. P. Ferris, S. P. Sherman, C. R. Thomas, J. Lu, A. D. Pyle, J. I. Zink and F. Tamanoi, *Small,* 2013, **9,** 697-704.
13 Y. L. Wang, Q. X. Wu, K. K. Sui, X. X. Chen, J. Fang, X. F. Hu, M. H. Wu and Y. F. Liu, *Nanoscale,* 2013, **5,** 4737-4743.
14 K. T. Thurn, H. Arora, T. Paunesku, A. G. Wu, E. M. B. Brown, C. Doty, J. Kremer and G. Woloschak, *Nanomedicine,* 2011, **7,** 123-130.
15 B. D. Chithrani, A. A. Ghazani and W. C. W. Chan, *Nano Lett.,* 2006, **6,** 662-668.
16 O. Lunov, V. Zablotskii, T. Syrovets, C. Rocker, K. Tron, G. U. Nienhaus and T. Simmet, *Biomaterials,* 2011, **32,** 547-555.
17 D. Guarnieri, A. Guaccio, S. Fusco and P. A. Netti, *J. Nanopart. Res.,* 2011, **13,** 4295-4309.
18 A. Lankoff, W. J. Sandberg, A. Wegierek-Ciuk, H. Lisowska, M. Refsnes, B. Sartowska, P. E. Schwarze, S. Meczynska-Wielgosz, M. Wojewodzka and M. Kruszewski, *Toxicol. Lett.,* 2012, **208,** 197-213.
19 Y. Liu, F. Jiao, Y. Qiu, W. Li, F. Lao, G. Q. Zhou, B. Y. Sun, G. M. Xing, J. Q. Dong, Y. L. Zhao, Z. F. Chai and C. Y. Chen, *Biomaterials,* 2009, **30,** 3934-3945.
20 R. Y. Prasad, S. Q. Simmons, M. G. Killius, R. M. Zucker, A. D. Kligerman, C. F. Blackman, R. C. Fry and D. M. DeMarini, *Environ. Mol. Mutagen.,* 2014, **55,** 336-342.
21 K. Wittmaack, *Chem. Res. Toxicol.,* 2011, **24,** 150–158.
22 B. Trouiller, R. Reliene, A. Westbrook, P. Solaimani and R. H. Schiestl, *Cancer Res.,* 2009, **69,** 8784-8789.
23 R. Anselmann, *J. Nanopart. Res.,* 2001, **3,** 329-336.
24 M. C. Bernier, K. El Kirat, M. Besse, S. Morandat and M. Vayssade, *Colloid Surf. B-Biointerfaces,* 2012, **90,** 68-74.
25 I. Pujalte, I. Passagne, B. Brouillaud, M. Treguer, E. Durand, C. Ohayon-Courtes and B. L'Azou, *Part. Fibre Toxicol.,* 2011, **8,** 16.
26 D. B. Warheit, R. A. Hoke, C. Finlay, E. M. Donner, K. L. Reed and C. M. Sayes, *Toxicol. Lett.,* 2007, **171,** 99-110.
27 K. Adachi, N. Yamada, K. Yamamoto, Y. Yoshida and O. Yamamoto, *Nanotoxicology,* 2010, **4,** 296-306.
28 Z. Magdolenova, D. Bilanicova, G. Pojana, L. M. Fjellsbo, A. Hudecova, K. Hasplova, A. Marcomini and M. Dusinska, *J. Environ. Monit.,* 2012, **14,** 3306-3306.
29 G. J. Nohynek and E. K. Dufour, *Arch. Toxicol.,* 2012, **86,** 1063-1075.
30 E. Fabian, R. Landsiedel, L. Ma-Hock, K. Wiench, W. Wohlleben and B. van Ravenzwaay, *Arch. Toxicol.,* 2008, **82,** 151-157.
31 R. Garcia-Contreras, R. J. Scougall-Vilchis, R. Contreras-Bulnes, Y. Ando, Y. Kanda, Y. Hibino, H. Nakajima and H. Sakagami, *In Vivo,* 2014, **28,** 209-215.
32 S. BaoYong, G. Wei, W. ShuQi, X. Feng and L. TianJian, *Compos. B, Eng.,* 2011, **42,** 2136-2144.
33 I. Fenoglio, J. Ponti, E. Alloa, M. Ghiazza, I. Corazzari, R. Capomaccio, D. Rembges, S. Oliaro-Bosso and F. Rossi, *Nanoscale,* 2013, **5,** 6567-6576.
34 Z. Li, X. B. Pan, T. L. Wang, P. N. Wang, J. Y. Chen and L. Mi, *Nanoscale Res. Lett.,* 2013, **8,** 7.
35 M. Simon, P. Barberet, M. H. Delville, P. Moretto and H. Seznec, *Nanotoxicology,* 2011, **5,** 125-139.
36 L. M. Jakubek, S. Marangoudakis, J. Raingo, X. Y. Liu, D. Lipscombe and R. H. Hurt, *Biomaterials,* 2009, **30,** 6351-6357.
37 M. A. Cousin, H. Hurst and D. G. Nicholls, *Neuroscience,* 1997, **81,** 151-161.
38 S. Makihira, H. Nikawa, M. Kajiya, T. Kawai, Y. Mine, E. Kosaka, M. J. B. Silva, K. Tobiume and Y. Terada, *Eur. J. Pharmacol.,* 2011, **670,** 409-418.

39 S. P. Yu, *Prog. Neurobiol.,* 2003, **70,** 363-386.
40 I. Lynch and K. A. Dawson, *Nano Today,* 2008, **3,** 40-47.
41 M. P. Monopoli, C. Aberg, A. Salvati and K. A. Dawson, *Nat. Nanotechnol.,* 2012, **7,** 779-786.
42 P. M. Kelly, C. Aberg, E. Polo, A. O'Connell, J. Cookman, J. Fallon, Z. Krpetic and K. A. Dawson, *Nat. Nanotechnol.,* 2015, **10,** 472-479.
43 D. Walczyk, F. Baldelli Bombelli, M. P. Monopoli, I. Lynch and K. A. Dawson, *J. Am. Chem. Soc.,* 2010, **132,** 5761–5768.
44 M. Horie, K. Fujita, H. Kato, S. Endoh, K. Nishio, L. K. Komaba, A. Nakamura, A. Miyauchi, S. Kinugasa, Y. Hagihara, E. Niki, Y. Yoshida and H. Iwahashi, *Metallomics.,* 2012, **4,** 350-360.
45 M. Horie, K. Nishio, K. Fujita, S. Endoh, A. Miyauchi, Y. Saito, H. Iwahashi, K. Yamamoto, H. Murayama, H. Nakano, N. Nanashima, E. Niki and Y. Yoshida, *Chem. Res. Toxicol.,* 2009, **22,** 543-553.
46 S. Sirnes, A. Kjenseth, E. Leithe and E. Rivedal, *Biophys. Res. Commun.,* 2009, **382,** 41-45.
47 F. R. Deng, P. Olesen, R. Foldbjerg, D. A. Dang, X. B. Guo and H. Autrup, *Nanotoxicology,* 2010, **4,** 186-195.
48 N. Ale-Agha, C. Albrecht and L. O. Klotza, *Biol. Chem.,* 2010, **391,** 1333-1339.
49 Q. S. Mu, N. S. Hondow, L. Krzeminski, A. P. Brown, L. J. C. Jeuken and M. N. Routledge, *Part. Fibre Toxicol.,* 2012, **9,** 11.
50 M. Stepnik, J. Arkusz, A. Smok-Pieniazek, A. Bratek-Skicki, A. Salvati, I. Lynch, K. A. Dawson, J. Gromadzinska, M. H. De Jong and K. Rydzynski, *Toxicol. Appl. Pharmacol.,* 2012, **263,** 89-101.
51 Z. M. Tao, B. B. Toms, J. Goodisman and T. Asefa, *Chem. Res. Toxicol.,* 2009, **22,** 1869-1880.
52 I. S. Kim, M. Baek, S. J. Choi, *J. Nanosci. Nanotechnol.,* 2010, **10,** 3453-3458.
53 Z. C, Wei, L. M. Chen, D. M. Thompson and L. D. Montoya, *J. Exp. Nanosci.,* 2014, **9,** 625-638.
54 J. Llop, I. Estrela-Lopis, R. F. Ziolo, A. Gonzalez, J. Fleddermann, M. Dorn, V. G. Vallejo, R. Simon-Vazquez, E. Donath, Z. G. Mao, C. Y. Gao and S. E. Moya, *Part. Part. Syst. Charact.,* 2014, **31,** 24-35.
55 M. J. Ware, B. Godin, N. Singh, R. Majithia, S. Shamsudeen, R. E. Serda, K. E. Meissner, P. Rees and H. D. Summers, *ACS Nano,* 2014, **8,** 6693-6700.
56 J. C. Phillips, R. Braun, W. Wang, J. Gumbart, E. Tajkhorshid, E. Villa, C. Chipot, R. D. Skeel, L. Kale and K. Schulten, *J. Comput. Chem.,* 2005, **26,** 1781-1802.
57 W. Humphrey, A. Dalke and K. Schulten, *J. Mol. Graph.,* 1996, **14,** 33-38.
58 A. D. MacKerell, D. Bashford, M. Bellott, R. L. Dunbrack, J. D. Evanseck, M. J. Field, S. Fischer, J. Gao, H. Guo, S. Ha, D. Joseph-McCarthy, L. Kuchnir, K. Kuczera, F. T. K. Lau, C. Mattos, S. Michnick, T. Ngo, D. T. Nguyen, B. Prodhom, W. E. Reiher, B. Roux, M. Schlenkrich, J. C. Smith, R. Stote, J. Straub, M. Watanabe, J. Wiorkiewicz-Kuczera, D. Yin and M. Karplus, *J. Phys. Chem. B,* 1998, **102,** 3586-3616.
59 W. L. Jorgensen, J. Chandrasekhar, J. D. Madura, R. W. Impey and M. L. Klein, *J. Chem. Phys.,* 1983, **79,** 926-935.
60 L. Jian, W. Chunlei, G. Pan, S. Guosheng and F. Haiping, *J. Chem. Phys.,* 2013, **139,** 234703 (8 pp.)-234703 (8 pp.).

The table of contents entry

Excess nanoparticles on the cell surface hindering ion exchange and disrupting exocytosis processes are the major trigger of cytotoxicity.